Electroencephalography and clinical Neurophysiology, 1985, 62: 32–44
Elsevier Scientific Publishers Ireland, Ltd.

TWO BILATERAL SOURCES OF THE LATE AEP AS IDENTIFIED BY A SPATIO-TEMPORAL DIPOLE MODEL

M. SCHERG and D. VON CRAMON

Max Planck Institute for Psychiatry, Department of Neuropsychology, D8000 Munich 40 (F.R.G.)

(Accepted for publication: July 19, 1984)

The origin of the late components of the auditory evoked potentials (AEPs) in the 60–250 msec range is still a topic of controversy. The midline maximum of the N100–P200 complex at frontocentral electrodes seemed to suggest an origin in the frontal lobe (review in Picton et al. 1974) or generation in a widespread diffuse cortical source (Wolpaw and Penry 1975). But, from their first detailed study on AEP scalp distribution, Vaughan and Ritter (1970) concluded that the orientation of the primary auditory cortex can account for the 'vertex response,' because of the summation of the fields of both temporal lobes. This view has been supported by evoked magnetic field measurements, showing vertically oriented dipoles located close to both Heschl's gyri and corresponding to the electric N100 activity (Elberling et al. 1982). Additional activity over the temporal lobes, occurring 25–30 msec after N100 (Kooi et al. 1971), was attributed to sources in the secondary auditory cortex (Wolpaw and Penry 1975). Describing even more phenomenological peaks, latency shifts and instability of scalp maps in the 60–250 msec AEP period, Wood and Wolpaw (1982) did not differentiate primary and secondary cortical sources, while Vaughan et al. (1980) extended their earlier view by attributing P245 and, partly, N150 and N220 to sources in the lateral surface of the superior temporal gyrus. More recently, in 'a reinterpretation' of the temporal AEP component, Peronnet et al. (1984) suggested an origin in precentral motor cortex.

Most of this controversy concerns the activity attributed to the reference electrode (Kooi et al. 1971; Wolpaw and Wood 1982) or the selection of particular electrode sites, which are assumed to register activity of only one source, thus enabling the overlap by other sources to be separated by correlation techniques (Wolpaw and Penry 1975; Peronnet et al. 1984).

The many open questions seemed to warrant a more basic study of the spatio-temporal overlap underlying the AEP. Therefore, the present study starts off by applying and extending the concepts developed for the propagation of intracranially evoked electric fields to the surface (Lorente de Nó 1947; Rush and Driscoll 1968; Plonsey 1969; Brody et al. 1973; Kavanagh et al. 1978; Ary et al. 1981; Vaughan 1982; Wood 1982). This results in a spatio-temporal dipole model, which can predict and analyse the scalp potential wave forms at any scalp location. Thus, simulations of AEP wave forms in the 60–250 msec range and analyses of reported data are presented, which were used to test different hypotheses on the generation of the late AEP.

Basis of spatio-temporal dipole model

By electric field theory, scalp potentials result from the superposition of the electrostatic fields of all charges within the brain. The electrostatic view is valid because capacitive and inductive effects can be neglected in the EP frequency range (Plonsey 1969). The net charge in the brain being zero, only pairs of positive and negative charges exist, each producing a dipole field (Vaughan 1974). Thus, the scalp potentials result from the superposition of the far fields of many microscopic, physical, dipoles. In the prestimulus interval, the resultant mean in the orientation of the

microscopic dipoles must be zero, on average, because their far fields cancel. In the poststimulus epoch synchronous changes occur in the orientation of numerous microscopic dipoles within the stimulated neural substrate, which may be viewed as consisting of a number of neural subsets, each having a small spatial extent as compared to head size. Only those subsets which exhibit a predominant orientation of neural elements will lead to a non-zero external field (Vaughan 1974) and each of these far fields may be approximated by the field of an equivalent, mathematical, dipole.

The accuracy of this mathematical approximation depends on the net distribution of charge in the local volume and its size as compared to the distance of the measuring probe (Feynman 1963). The smaller the local volume, the better is the conformity in location of physical and equivalent dipoles. Real surface potentials may, therefore, be closely modelled by the spatio-temporal superposition of a finite number of such equivalent dipoles, provided a sufficient subdivision into local subsets is made. It is important to realize that this view of multiple local activities, each having individual spatial and temporal properties, differs substantially from the attempt to describe the instantaneous scalp potential distribution by the field of a single dipole without spatial constraints (Wood 1982).

When this multiple dipole concept is applied to the EP source problem two tasks remain: first, the number of dipoles and their spatio-temporal characteristics must be determined, which are necessary to describe fully the potential at any location on the scalp and at any instant. Secondly, location, orientation and temporal properties of these equivalent dipoles must be related to the physiology of the underlying neuroanatomical substrate.

According to the mechanisms of far-field generation outlined above, a spatio-temporal dipole model (STDM) was conceived on the basis of the following assumptions.

(1) The neural substrate generating the surface EP can be defined as consisting of a limited number of neural subsets (generators), such that each is localized within a small volume as compared to head size.

(2) The external far field of each neural subset adds linearly to the scalp potential according to the laws of electrostatics (spatio-temporal superposition).

(3) The spatial properties, i.e., the scalp potential distribution associated with each generator, can be approximated by the field of an equivalent dipole located within or in close proximity to the neural substrate. Location and orientation of each dipole are stationary, as is the spatial organization of the underlying neural structure.

(4) The temporal properties of each generator are reflected in the magnitude of the equivalent dipole, which is assumed to be a continuous function of time described by an onset latency and several peaks following. The temporal course of dipole magnitude is thought to depict the compound discharge processes of the underlying structure.

Given these assumptions, both prediction and analysis of surface potential wave forms can be accomplished, considering:

(a) The forward problem: given a certain hypothesis on location, orientation and temporal course of compound activity of one or more (n) generators, the potential wave forms on the scalp can be predicted by superimposing the dipolar fields of all generators according to:

$$u_k(t) = \sum_{i=1}^{n} m_i(t) \cdot d(\vec{r}_i, \zeta_i, \alpha_i; \vec{e}_k)$$

where $u_k(t)$ is the potential wave form at electrode k, $m_i(t)$ is the temporal function of dipole magnitude (scaled in surface voltage units) and d is the dipole function predicting the relative amplitude at electrode k as defined by the location ($\vec{r}_i$), of the i'th generator and its spatial orientation (ζ_i, α_i) relative to electrode location ($\vec{e}_k$). The actual dipole function used depends on the choice of a particular head model.

(b) The inverse problem: given a set of potential wave forms measured at different scalp electrodes, location, orientation and wave form parameters of the equivalent dipoles are determined by a least squares fitting procedure minimizing the difference between measured and model-predicted wave forms for all derivations simultaneously. A mathematically unique solution can be found only for a small number of dipoles, limited by the

degrees of freedom and the accuracy of the measured signals. In a stepwise procedure, configurations of an increasing number of dipoles, exhibiting consecutively more degrees of freedom in spatial parameters and temporal activity (mono-, bi- or triphasic wave form), can be tested. As a goodness of fit criterion, similar to rho defined by Schneider (1972), the relative deviation variance (RDV) can be used, which is given by the total variance in the difference wave forms between measured and model data divided by the total variance of the measured data (Scherg 1984). Accordingly, different hypotheses concerning the number and configurations of sources can be ranked.

(c) The reference electrode problem: the comparison of predicted and measured wave forms is not dependent on the choice of a particular reference, because the potential differences to the reference electrode can be calculated by subtracting $u_{ref}(t)$ from $u_k(t)$ and by using these potential differences for the model fit (Schneider 1972). To avoid bias, i.e., an overweight of signal and noise at the reference electrode, in the fitting process the average reference is preferable (Scherg and Von Cramon 1984).

Methods

Simulation of surface potential wave forms

For the prediction of the wave forms recordable along a coronal chain of electrodes the location and moment of each dipole were assumed to lie within the coronal plane, defined by horizontal x- and vertical z-axes. Thus, in this 2-dimensional case, the 3 variable spatial parameters were eccentricity (r) and angle (ϑ), for location, and angle (α) against the z-axis for the orientation of a dipole. Magnitude and temporal course of dipole strength were defined by the 2 amplitudes of a biphasic discharge pattern and by the peak, on- and offset latencies, as indicated by arrows and vertical bars, for amplitudes, in the temporal pattern of dipole A in Fig. 1. Continuity of this 6-parametric pattern was achieved by using spline functions with flat on- and offset connecting onset, peak and offset points.

Spline functions were chosen because they provided a smooth connection between these 4 time/amplitude points while allowing for fast computation. Simpler or more complex local wave form patterns could be simulated by using less or more temporal parameters (e.g., 4 for a monophasic or 8 for a triphasic pattern). The overall latency of the biphasic pattern was defined by the latency of the first peak. A second source could be simulated, in the simplest case, by a similar biphasic pattern differing only in latency and in amplitudes, apart from spatial differences, e.g., dipole B in Fig. 1. An independent parametrization of multiple dipoles in the coronal plane, each having a particular biphasic course of dipole strength, required 9 spatio-temporal parameters for each dipole, i.e., 18 for 2 sources. This number can be considerably reduced by assuming bilateral symmetry of location (only 16 parameters needed for a pair of dipoles) or similarity of wave shape (12 if only peak latency, relative magnitude and orientation are to be independent). The assumption of bilateral symmetry in location was justified by the observation that changes in location of less than 0.1*head radius were almost without influence on scalp distribution, particularly for tangential dipoles.

Reference-free potential wave forms at 13 electrodes equally spaced between left ($-120°$ to z-axis) and right mastoids ($+120°$) were calculated in 3 steps. First, the relative contribution of each dipole at any electrode was calculated according to the 3-shell head model approach by Ary et al. (1981). This implied evaluation within the homogeneous spherical head model (Brody et al. 1973) with subsequent transformation of eccentricity (Scherg 1984) by:

$$r(\text{3-shell}) = r(\text{homog})*\left(1.627 - 0.67*r(\text{homog})^{2.3}\right)$$

This step corresponds to calculating a scalp map for each dipole from its spatial parameters and yields a weight factor for each electrode-dipole combination. Secondly, the pattern of dipole strength, as determined from the 6 temporal/amplitude parameters, was multiplied with the appropriate electrode weight factors to produce the single dipole wave forms at each electrode (Fig. 1A and B). Thirdly, the final wave form at each

electrode was obtained by summing up the wave forms contributed by each dipole (e.g. Fig. 1, bottom).

Analysis of recorded surface potentials

For source analysis, records with a high signal-to-noise ratio were required. Because grand average AEP data published by Peronnet et al. (1974) and Vaughan et al. (1980) fulfil this requirement, AEP wave forms from both papers, as recorded along a coronal chain of electrodes, were digitized on a graphic tablet after photographic magnification (470 or 615 points). Only the first 525 (405) msec, 100 msec pre-stimulus time included, of each wave form were analysed and represented by 50 equidistant interpolated amplitude values for further computation. Each set of scalp records was linearly transformed to average reference for analysis (Scherg and Von Cramon 1984). The 13 coronal electrodes were assigned to spatial coordinates identical to those in the model simulation while the nose electrode was assigned to an angle of 95° to the z-axis in the sagittal (y-z) plane, with the z-axis pointing at 2 cm in front of Cz. According to these electrode positions the head model was projected onto a coronal brain section (Nieuwenhuys et al. 1978, Fig. 36) with the centre approximately 1 cm below the posterior commissure and a head radius of 8.4 cm.

The least squares fit procedure by Deuflhard and Apostolescu (1980) was used to minimize the difference between recorded and model wave forms simultaneously at all electrodes throughout the whole recording interval (at a total of $14*50 = 700$ points) by iterative adjustment of the model parameters described above. Starting values of dipole location, orientation and temporal pattern were set according to the hypothesis tested. Individual parameters could be held constant for studying the effects on wave form by other parameters. It should be noticed that by this inverse spatio-temporal approach not only the coordinates of dipole location and orientation are obtained, but also the latencies and amplitudes of the temporal pattern of each dipole.

Results

(A) Prediction of scalp potential wave form

The conceptual steps leading to the prediction of surface wave form are illustrated in Fig. 1. Each dipole (A or B) produced a scalp potential distribution specific to its location and orientation, if viewed independently. Depicted as a scalp map of relative amplitudes this distribution of a single fixed dipole was stationary, with equipotential lines indicating the relative contribution at each electrode. The temporal course of activity associated with each dipole, as defined by the 4 latencies and 2 amplitudes of the biphasic pattern of dipole strength on the left, projected to each electrode with identical shape but different amplitudes according to the factors given by the scalp map. Thus, the electrodes lying near the positive end of the dipole registered the largest positive field contribution, whereas the electrodes facing the other end registered an inverted wave form, being smaller in amplitude because of their larger distance from the dipole in the examples shown. The lateral, more radially oriented, dipole B was defined with a wave shape similar to dipole A, except for increased latency and decreased amplitude (1/2) of the whole pattern. Yet, the lateral potential maximum was found to be of almost identical size to that of the more tangential dipole A. Also, from the scalp maps of dipoles A and B, small contributions at the contralateral mastoid, minimal ones at the nose and considerable interference at sternovertebral electrode sites were predicted.

If temporal overlap of two or more dipoles, exhibiting asynchronous activation, was simulated, the scalp distribution could no longer be described by a unique scalp map, because there was a continuous change in relative dipole magnitude (Fig. 2). In contrast, description by 2 dipoles with different temporal courses of activity was sufficient to produce remarkable changes of wave form across different scalp locations when their fields were superimposed (Fig. 1, bottom). For example, a triphasic pattern resulted at the mastoid electrodes despite the similar biphasic patterns of both sources, the latency of the first positive peak increased from the vertical to the lateral electrodes, while the latency of the corresponding

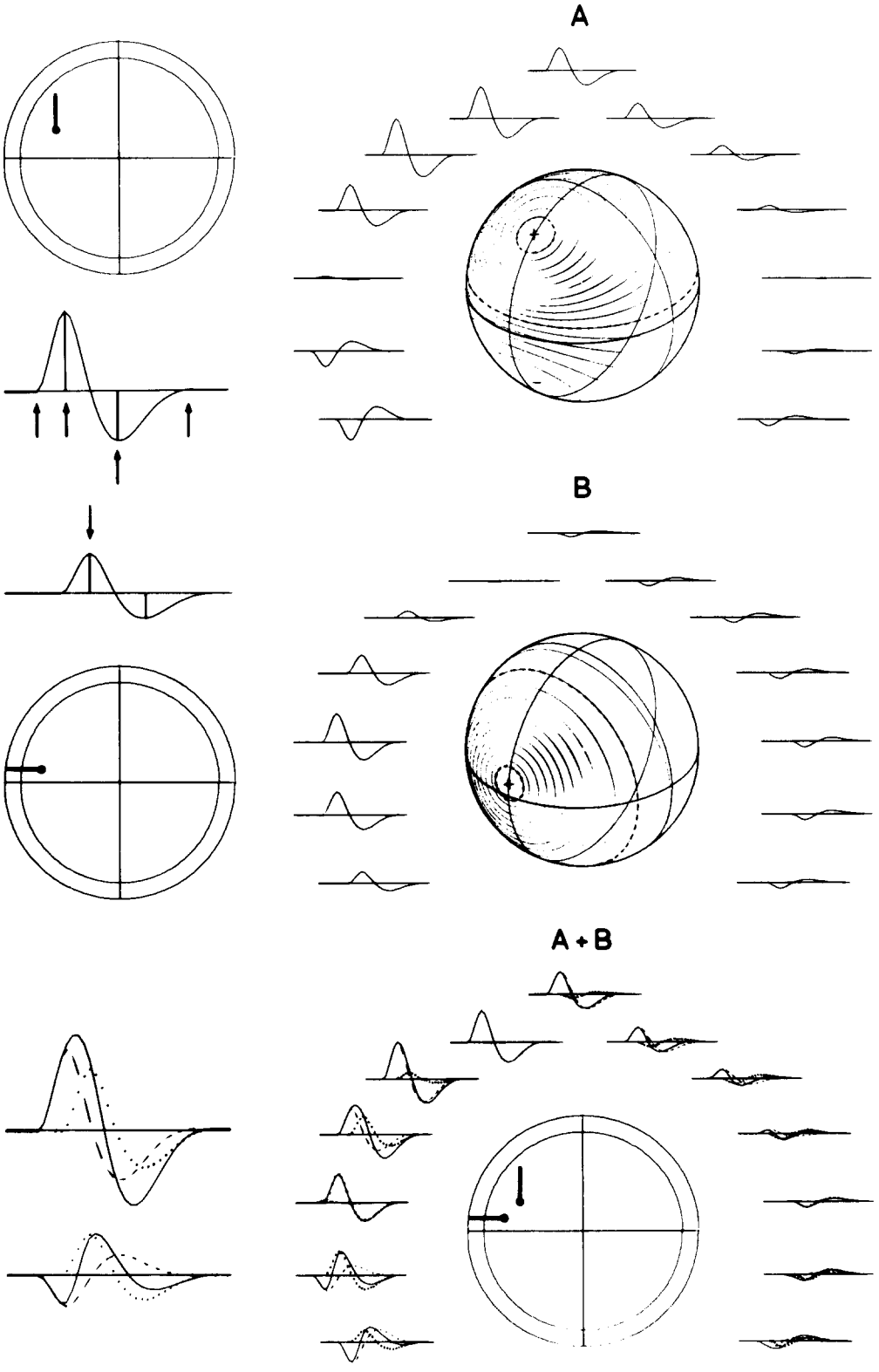
A
B
A + B

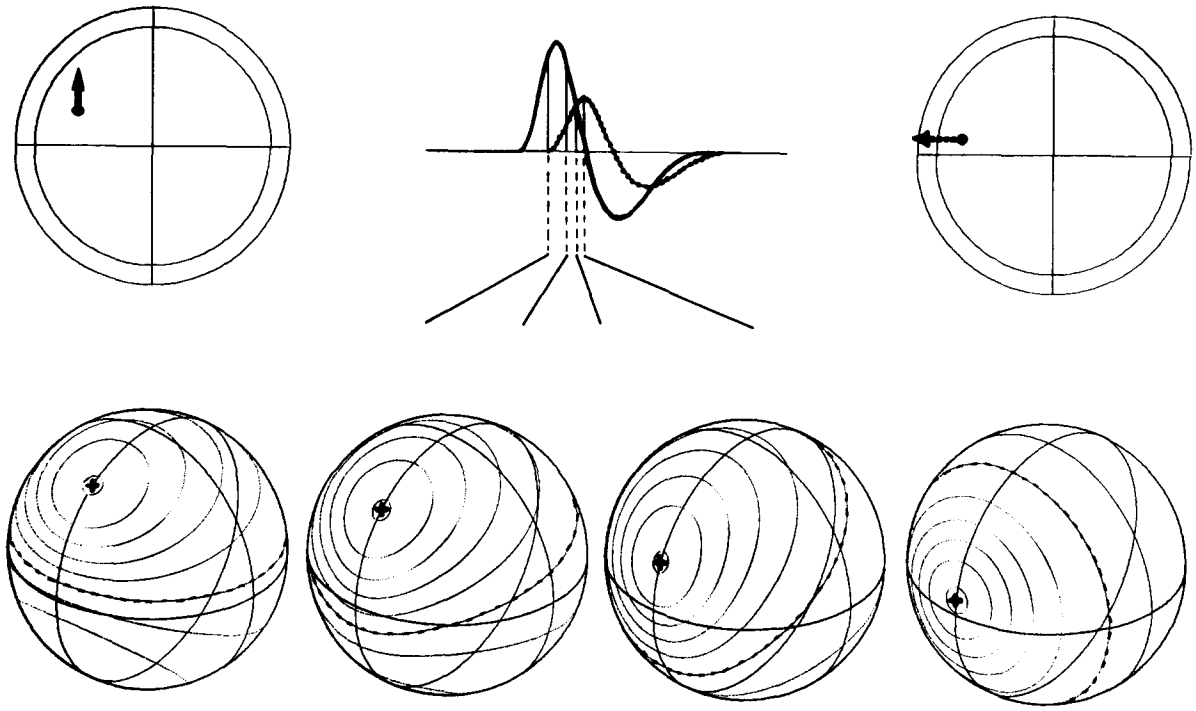

Fig. 2. Instantaneous scalp maps in the case of spatio-temporal overlap. Four time instances selected, which correspond to different relative strengths of dipole A (left, full curve) and dipole B (right, dotted curve): 100/0%, 75/25%, 50/50%, 0/100% from left. Diagrams as in Fig. 1, only 20% equipotential lines shown. Note the variation in peak location over time giving the appearance of a moving dipole. Only a minimal part of the whole range of instantaneous scalp maps occurring during the interval of overlap is shown.

negativity was shorter at the mastoid and the first peak markedly broadened around C3. Apparently the superposition of different source activities introduced a high complexity into the scalp potential wave forms, thus making the determination of a particular scalp map at instances of maximal field power or at prominent peaks questionable. In comparison to the large number of degrees of freedom inherent in a single instantaneous scalp map, only 6 spatial and 8 temporal parameters were necessary to simulate these wave form changes along a coronal chain of electrodes as well as a small subset of related scalp maps (Fig. 2).

An example of the wave forms predicted for bilateral sources is given in Fig. 3. If a second dipole was located contralateral to dipole A with symmetric location and orientation and an identical synchronous activity, a symmetric scalp distri-

Fig. 1. Prediction of the scalp potentials due to vertical (A) and horizontal (B) dipoles along a coronal chain of electrodes connecting both mastoids (120% to vertical z-axis in head model). The spherical 3-shell head model diagrams (inner circle equivalent to dura; skull–scalp border not shown) depict location (dot) and orientation (dash) of dipoles in a frontal view. The scalp maps give a 3-dimensional rotated view of relative amplitude distribution, indicated by 10% equipotential lines (0 and 95% dashed), with the tilted ellipse indicating the coronal plane, crossing the sagittal plane on the top and the horizontal plane laterally near the maximum of dipole B. The coronal wave forms result from multiplying the temporal pattern of dipole strength (left) with the relative amplitude factor according to electrode location in the scalp map. The temporal pattern is defined by the latencies (arrows) and amplitudes as illustrated for dipole A. Dipole B differs only in peak latency (arrow) and relative amplitude of the temporal pattern. The wave forms due to spatio-temporal overlap of dipoles A + B are shown in the bottom tier. The overlap at electrodes 2 and 4 (counting from right mastoid) is depicted on a larger scale on the left (dashed curves: dipole A; dotted: dipole B). Note, that at electrode 3 mainly the lateral dipole is contributing and at electrode 5 the vertical dipole.

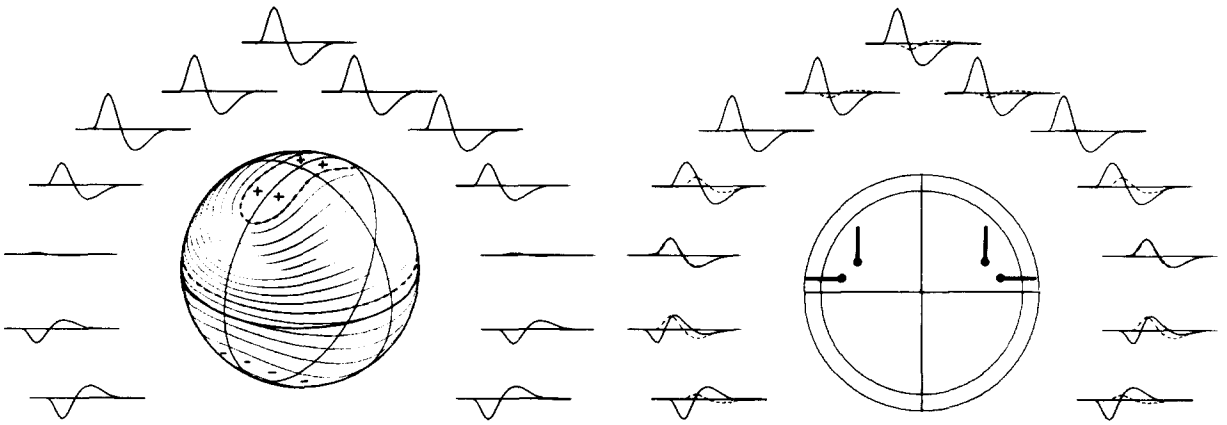

Fig. 3. Simulation of coronal wave forms due to bilateral dipoles. Synchronous activity of both vertical dipoles results in a stationary scalp map of relative amplitudes (left) showing a broad vertex maximum and zero potential over temporal regions. Addition of a second bilateral symmetric source (as dipole B in Fig. 1), allowed no longer description by a single scalp map and led to marked wave form changes, while retaining bilateral symmetry. Dashed lines illustrate contribution to wave form by horizontal dipoles (right). Note that there is no 'indifferent electrode' site in the coronal plane.

bution resulted, with a broad vertex maximum (Fig. 3, left). If one pattern was peaking earlier than the other, this vertex maximum would first tilt to the earlier peaking side and then to the opposite, thus inducing the image of a moving dipole. Similarly, if a second bilateral symmetric source was activated subsequent to the first (temporal course as of dipole B in Fig. 1), there was no unique map accounting for the wave form changes seen in the symmetrically distributed potentials from vertex to either mastoid (Fig. 3, right). The prediction of these wave forms for the whole recording interval was based on only 14 spatio-temporal parameters due to the symmetry restrictions. If independence of the orientations, onset latencies and amplitudes of the biphasic patterns of all 4 dipoles was allowed, a total of 23 free parameters permitted simulation of the effects of interhemispheric differences in latency, magnitude and orientation of 2 bilateral sources at arbitrary locations within the head model.

Analysis of scalp recorded AEPs

A first attempt to explain the scalp topography of late AEPs, reported by Vaughan et al. (1980, pg. 281, Fig. 1, top), by a single dipole with a biphasic pattern representing the N100–P200 complex gave a poor fit (Table I) of wave form at both vertical and lateral electrodes. In the next step, a single bilateral source was hypothesized and the eccentricity yielding best wave form fit was determined. The resultant location (Fig. 4,

TABLE I

Stepwise test of source hypotheses (data by Vaughan et al. 1980).

Step	N of sources/dipole		IP wave form	N par	RDV (%)	DRDV (%)
1	1 central	1	–	9	11	–
2	1 bilateral	2	–	10	7.0	4.0
3	1 bilateral	2	to, relat. A	12	6.9	0.1
4	2 bilateral	4	to, relat. A	20	4.1	2.8
5	2 bilateral	4	to, all A	23	2.6	1.5
6	2 bilateral	4	all t, all A	32	2.2	0.4

IP wave form, independent wave form parameters for each dipole; N par, total number of spatio-temporal parameters required; RDV, relative deviation variance; DRDV, decrease in RDV by actual step; to, onset latency; A, amplitude.

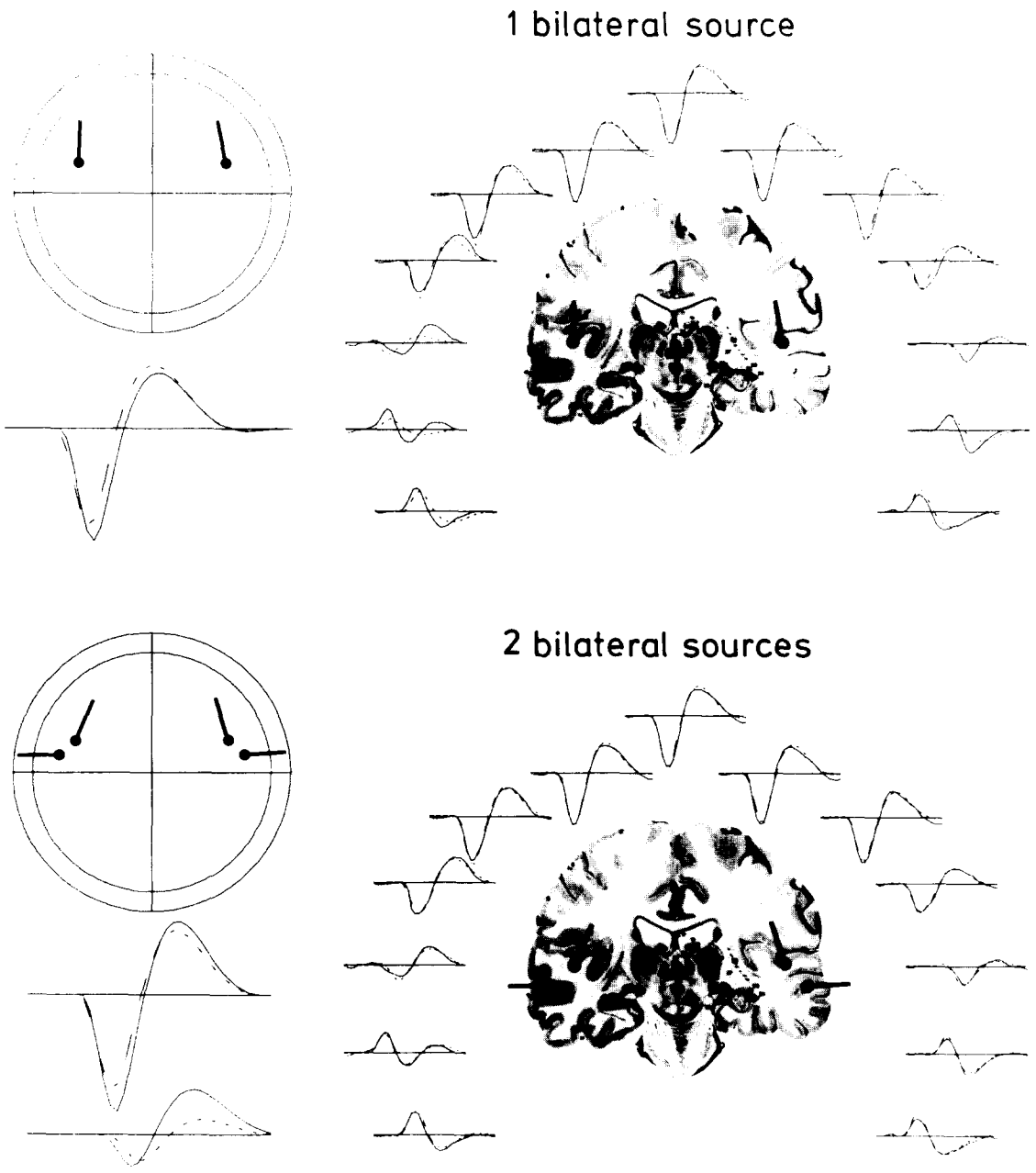

Fig. 4. Spatio-temporal analysis of AEP data published by Vaughan et al. (1980). Full lines (on right) show the coronal wave forms as digitized from their Fig. 1 (read condition). Recorded and model wave forms (dashed lines) are referred to the nose (positivity upwards). 20 msec pre- to 360 msec poststimulus interval shown. The patterns of temporal activity are plotted on the left, as in Fig. 1, for the vertical dipoles (N100/P180, top and bottom, upper pair of curves) and horizontal dipoles (N130/P210, bottom pair of curves). Right and left hemispheric activity indicated by full (dashed) curves. The second bilateral source of horizontal dipoles, having delayed and reduced activity, explains the deviations in wave form and latency over temporal sites not described by the N100/P180 activity of the vertical dipoles (top). Note the excellent fit of reported and model wave forms by only two bilateral, symmetrically located, sources (bottom right). The dipole solutions were projected onto a coronal brain section (modified from Nieuwenhuys et al. 1978, by permission) to illustrate their location within the temporal lobes and their orientation perpendicular to the cortical surface.

TABLE II

Spatio-temporal parameters obtained for 2 bilateral sources.

Peak		Vertical source		Lateral source	
		N100	P180	N130	P210
Rel. latency	A	101/99	190/188	124/138	210/224
(msec)	B	94/106	167/182	138/137	212/210
Rel. amplitude	A	100/82	63/55	26/22	39/13
(%)	B	100/94	68/51	21/20	8/14
Eccentricity	A	0.60		0.68	
(unit radius)	B	0.48		0.70	
Theta	A	+−67		+−79	
(degrees)	B	+−64		+−73	
Alpha	A	−24/+17		−92/+86	
(degrees)	B	−21/+20		−66/+85	

A: Vaughan et al., 1980; B: Peronnet et al. 1974. Values of right/left hemisphere given, when independent. Latencies referred to mean N100 at 100 msec, amplitudes to right hemisphere N100. Theta, location angle; alpha, orientation angle to vertical z-axis.

top) within the temporal lobe was almost identical to that of the vertical dipoles in the final solution (Fig. 4, bottom). Yet, the lateral wave forms were still poorly explained, thus requiring the assumption of further sources. Because the observed deviations of measured and model wave forms were of equal polarity on both sides, at least a second bilateral source was required, exhibiting a later onset latency and different relative amplitudes. The best fit obtained with this 4 dipole hypothesis, with symmetric location, was able to model the recorded signals in almost every single deflection at any single electrode (Fig. 4, bottom), leaving only a minor part of the wave form unexplained (Table I). In addition, this solution with 2 bilateral sources produced a high symmetry of orientation for each pair of dipoles. Further, the spatio-temporal parameters (Table II), obtained by the fitting procedure, provided a direct estimate of the latency and magnitude of the activity contributed by each dipole. Allowing for full independence of the wave forms, i.e., in timing of peaks, on- and offset, of each dipole did not substantially improve the fit (Table I), nor had this a sizable influence on dipole location, orientation or temporal course of activity.

To test further the validity of the 2 bilateral source solutions, the left ear grand average AEPs by Peronnet et al. (1974, Fig. 1) were similarly analysed. Again the best fit solution (RDV = 2.6%) yielded 2 pairs of bilateral dipoles with the vertical dipoles located more medially but still within the temporal lobe. Orientations and temporal courses of activity were highly similar to the results shown above (Table II). The temporal parameters indicated shorter latency and greater magnitude of the N100–P180 activity in the contralateral hemisphere. A preliminary analysis of the 7 coronal channels in the AEP distribution, recorded against a sterno-vertebral reference by Wood and Wolpaw (1982), showed comparable dipole results if complete bilateral symmetry of sources was assumed. Their restriction to unilateral scalp records necessitated this assumption.

Discussion

The present results fully support the hypothesis by Vaughan et al. (1980) that all AEP components, elicited by periodic stimulation, in the 60–250 msec range, can be explained by sources within the superior temporal plane and the lateral superior temporal gyrus. Both the eccentric location and the orientation of the best fitting dipoles are independent indices to this explanation. Accepting the

view of orthogonality between the orientation of the external dipole field and the generating cortical layers (Vaughan 1982), the observed dipole orientations, as well as their latency difference, suggest the subsequent activation of primary auditory cortex (vertical dipole perpendicular to superior temporal plane) and secondary auditory cortex (radial dipole perpendicular to lateral surface of the superior temporal gyrus). Further, the vertical dipoles are consistent both in location and orientation with magnetic evoked field results (Elberling et al. 1982). Yet the latency shift of the electric N100 can be seen to be much larger than that of the corresponding magnetic peak across different scalp locations, indicating the inability of the magnetoencephalogram to measure the radial part of the dipole field (Cohen and Cuffin 1983), which, for the AEP, should reflect activity predominantly from secondary auditory cortex.

By the results of both electric and magnetic evoked fields, it cannot be excluded that other more central or frontal structures also contribute to the 60–250 msec AEP. Particularly, a more wide-spread activation within or near the temporal lobe, e.g., posterior insula, should have little influence on the location of the equivalent dipoles, but possibly more on their orientation. Sources on the midline should have produced systematic deviations of model and measured wave forms, unless being highly synchronous with the vertical dipoles. But, in the latter case, a substantial contribution by such paramedian sources ought to be balanced by further eccentricity of the temporal dipoles. Adding a fifth dipole to the model and testing many locations and onset times as starting values in an analysis of the data by Vaughan et al. (1980) did not attribute more activity to this dipole (decrease in RDV less than 0.1%), than could be accounted for by residual noise in the digitized (or measured) data. Further, the wave forms for unilateral temporal sources (cf., Fig. 1) showed a clear asymmetry in the coronal plane, similar to that reported for patients with unilateral temporal lobe lesions (Peronnet et al. 1974; Michel and Peronnet 1982). Recently, Woods et al. (1984) reported a case of cortical deafness after bilateral temporal lobe lesions with preserved AEP components P1, N1 and N2. Careful inspection of the coronal wave forms presented revealed an asymmetric scalp distribution with larger amplitudes over the hemisphere having a 'new lesion,' while there was apparently no evidence for the temporal AEP component or for a latency increase from the vertex to the temporal electrodes, which can be seen in normals over both, and in patients only over the intact, temporal lobes (e.g., Michel and Peronnet 1982, their Fig. 8). Cortical deafness, in this case, may therefore be associated with a loss of the temporal AEP component. Considering all the evidence, we suggest that each of the 4 equivalent dipoles, obtained for the late AEP, does indeed have a close correspondence to the neuroanatomical substrate, seen in location, orientation and temporal course of the external field.

The spatio-temporal dipole model also illuminates the reference electrode problem. The nature of an intracranial dipole field implies that location and orientation of the dipole are uniquely defined by the potential gradients on the scalp (Fig. 1). Hence, there is no *a priori* need for a so-called 'indifferent' reference electrode, because the dipole coordinates can be determined from the potential differences to any common electrode (Schneider 1972). An additive shift of potential must be attributed to the monopolar field, i.e., to the potential difference between head and body, in other words to a non-cephalic reference. Search for an 'indifferent' electrode site in Fig. 1 revealed that any electrode on the zero-equipotential line of the dipole field A was indifferent to the transient activity of this dipole, but registered activity from dipole B, unless positioned also on the zero-potential line of dipole B. Evidently, if more than 2 sources are active during the analysis epoch, a common site of zero-reference no longer exists in general. From Figs. 1 and 3, the effects on the reportedly 'indifferent' nose (Vaughan 1974) and sterno-vertebral references (Kooi et al. 1971), as used for AEP registration, can be inferred. The nose electrode, positioned just below the crossing point of the mid-sagittal and horizontal planes and, accordingly, below the zero-potential line of dipole A, senses only about 10–20% of inverted activity due to the bilateral vertical dipoles, in contrast to more than 50% at the lower parts of the head model, corresponding to the area of

electrical connection to any non-cephalic 'reference.' Further, the largest field gradients of the bilateral vertical dipole A (Fig. 3) are seen over temporal sites. Although demonstrating a similar scalp distribution of AEP gradients (Wood and Wolpaw 1982), which could be fitted by an equivalent, vertically oriented, paramedian dipole (Wood 1982), these authors denied the large contribution of the 'vertex response' to their sterno-vertebral reference (Wolpaw and Wood 1982), postulated by Vaughan (1974) for vertical dipoles.

No other than the vertical component of a dipole can account for the AEP differences seen between vertex and lower scalp sites, because the horizontal components show isopotential at top and bottom of the head model, as can be deduced from the orthogonality of dipole orientation and planes defined by equipotential lines. A horizontal dipole, pointing to the nose, produces isopotential even throughout the coronal chain of electrodes (consider sagittal and coronal planes exchanged for dipole B in Fig. 1); this allowed the *a priori* restriction of orientation to within the coronal plane. Also, the changes due to a fronto-posterior deviation of dipole A was simulated by testing locations 15 mm in front of or behind the coronal plane. The potential distribution found was almost identical (RDV = 0.01%) to that of a dipole within the plane, exhibiting minimally decreased eccentricity (3.8%) and amplitude (4.2%). Thus, the *a priori* limitation to coronal plane dipoles was a legitimate reduction in the degrees of freedom for modelling the coronal AEP scalp distribution. The exact fronto-posterior location within a 15 mm range off the coronal plane, as seen in the magnetic evoked fields (Elberling et al. 1982), can only be determined by spatio-temporal analyses including more electrodes in a sagittal direction. Although we found evidence for earlier and greater activity in the hemisphere contralateral to stimulation (Table II; data by Peronnet et al. 1974), similar to the results of Elberling et al. (1982), the interpretation of hemispheric differences demands care, because the full 3-dimensional solution is needed to determine dipole strength accurately. Also, the geometry of the local substrate is an important determinant of equivalent dipole strength (Vaughan 1974), thus making simple conclusions about hemispheric contributions questionable.

The new spatio-temporal dipole model allows for direct and simultaneous evaluation of all wave forms across the scalp during the whole recording interval. It is not restricted to analysis of scalp maps at selected instants, as defined by peaks (Wood 1982), maximal field power (Lehmann and Skrandies 1980) or constancy in scalp distribution (Wood and Wolpaw 1982). The assumption underlying these approaches was that there are instants when the activity of one source is dominant or when the source configuration is stable. Thus, implicitly, the factor time was discarded, although being useful in tackling the superposition problem. In contrast, the new spatio-temporal dipole model includes time as an independent variable to dissolve temporal overlap by different sources. Accordingly, the separability of 2 or more overlapping sources is increased, because relying not only on differences in location and orientation, but also on temporal differences. Thus, the number of uniquely determinable parameters, and hence of dipoles, is no longer limited by the number of recording channels (Kavanagh et al. 1978), but mainly depends on the degrees of freedom in the recorded data set (Scherg 1984).

Further, the influence of noise on the dipole solution is considerably reduced by the requirement of continuous and smooth functions describing the temporal courses of activation. The choice of biphasic temporal patterns was based on the observation that separate monophasic dipoles underlying N100 and P180 had similar locations and orientations and required more parameters, thus increasing instability of the dipole solutions. On the other hand triphasic patterns were not needed or able to explain reported AEP wave forms with fewer dipoles.

The spatio-temporal approach may also help to understand the generation of other EPs which exhibit overlapping source activities, e.g., early (Scherg 1984) and middle latency auditory EPs and somatosensory EPs. In any case, the model allows a large set of wave forms to be condensed into few parameters. But, because the laws of electrostatic field propagation can be imposed by this model, the physiological significance of the

extracted parameters can be considerably enhanced as compared to purely phenomenological approaches, such as peak analysis or scalp mapping. Nevertheless, independent physiological evidence is needed to prove that a particular source model configuration obtained is the only solution consistent with the underlying physiology.

Summary

A new spatio-temporal dipole model is presented, which enables prediction and analysis of scalp potential wave forms due to spatio-temporal overlap of multiple generators. Each generator is thought to represent a local neural subset, the electric activity of which can be modelled by an equivalent dipole with stationary location and orientation closely related to the spatial organization of the neural subset. The temporal course of dipole magnitude is assumed to depict the external far field due to the compound discharge processes of the generator. Simulations of uni- and bilateral dipoles within the temporal lobe, oriented vertically and horizontally, demonstrate how spatio-temporal overlap mag bring about the 'vertex response' of the late AEP and the wave form changes observed over temporal sites.

Analyses of late AEPs reported for a coronal chain of electrodes by Peronnet et al. (1974) and Vaughan et al. (1980) revealed that the wave forms in the 60–250 msec range could be perfectly matched at all electrodes by model wave forms due to 2 bilateral sources within the temporal lobe. Their locations, orientations and their latency difference of about 30 msec suggest consistently that the sequential activation of primary and secondary auditory cortices is the predominant source to the late AEPs.

Résumé

Les 2 sources bilatérales de l'AEP tardif telles qu'elles sont identifiées par un modèle de dipôle spatio-temporel

On présente un nouveau modèle de dipôle spatio-temporel qui permet de prédire et d'analyser les formes d'onde de potentiels de scalp dues au chevauchement spatio-temporel de multiples générateurs. Chaque générateur est supposé représenter un sous-ensemble neuronal local dont l'activité peut être modélisée par un dipôle équivalent avec une localisation stationnaire et une orientation en relation étroite avec l'organisation spatiale du sous-ensemble neuronal. Le décours temporel de la grandeur du dipôle est supposé rendre compte du champ lointain externe dû aux processus de décharge complexe du générateur. La simulation de dipôles uni- et bilatéraux dans le lobe temporal, orientés verticalement et horizontalement, démontre comment le chevauchement spatio-temporel peut contribuer à la "réponse au vertex" de l'AEP tardif et des changements de forme d'onde observés aux sites temporaux.

Les analyses des AEP tardifs rapportées par une couronne d'électrodes par Peronnet et al. (1974) et Vaughan et al. (1980) révélèrent que les formes d'onde dans la bande 60–250 msec pouvaient être parfaitement simulées pour toutes les électrodes par un modèle de formes d'ondes dû à 2 sources bilatérales dans le lobe temporal. Leur localisation, leur orientation et leur différence de latence d'environ 30 msec suggèrent fortement que l'activation séquentielle des cortex auditifs primaire et secondaire est la source principale des AEP tardifs.

We are grateful to Michael Streit for writing the digitization program and to Victor Apostolescu for providing the least-squares-fit routines.

References

Ary, J.P., Klein, S.A. and Fender, D.K. Location of sources of evoked scalp potentials: corrections for skull and scalp thicknesses. IEEE Trans. biomed. Engng, 1981, 28: 447–452.

Brody, D.A., Terry, F.H. and Ideker, R.E. Eccentric dipole in a spherical medium: generalized expression for surface potentials. IEEE Trans. biomed. Engng, 1973, 20: 141–143.

Cohen, D. and Cuffin, B.N. Demonstration of useful differences between magnetoencephalogram and electroencephalogram. Electroenceph. clin. Neurophysiol., 1983, 56: 38–51.

Deuflhard, P. and Apostolescu, V. A study of the Gauss-Newton algorithm for the solution of nonlinear least squares

problems. In: J. Frehse, D. Pallaschke and U. Trottenberg (Eds.), Special Topics of Applied Mathematics. North-Holland Publ., Amsterdam, 1980: 129–150.

Elberling, C., Bak, C., Kofoed, B., Lebech, J. and Saermark, K. Auditory magnetic fields from the human cerebral cortex: location and strength of an equivalent current dipole. Acta neurol. scand., 1982, 65: 553–569.

Feynman, R.P. Lectures on Physics. Addison-Wesley, Palo Alto, CA, 1963.

Kavanagh, R.N., Darcey, T.M., Lehmann, D. and Fender, D.H. Evaluation of methods for three-dimensional localization of electrical sources in the human brain. IEEE Trans. biomed. Engng, 1978, 25: 421–429.

Kooi, K.A., Tipton, A.C. and Marshall, R.E. Polarities and field configurations of the vertex components of the human auditory evoked response: reinterpretation. Electroenceph. clin. Neurophysiol., 1971, 31: 166–169.

Lehmann, D. and Skrandies, W. Reference-free identification of components of checkerboard-evoked multichannel potential fields. Electroenceph. clin. Neurophysiol., 1980, 48: 609–621.

Lorente de Nó, R. Analysis of the distribution of action currents of nerve in volume conductors. Stud. Rockefeller Inst. med. Res., 1947, 132: 384–482.

Michel, F. et Peronnet, F. L'hémianacousie, un déficit auditif dans un hémisphère. Rev. neurol., 1982, 138: 657–671.

Nieuwenhuys, R., Voogd, J. and Van Huijzen, R. The Human Central Nervous System. Springer, Berlin, 1978.

Peronnet, F., Michel, F., Echallier, J.F. and Girod, J. Coronal topography of human auditory evoked responses. Electroenceph. clin. Neurophysiol., 1974, 37: 225–230.

Peronnet, F., Giard, M.-H., Bertrand, O. and Pernier, J. The temporal component of the auditory evoked potential: a reinterpretation. Electroenceph. clin. Neurophysiol., 1984, 59: 67–71.

Picton, T.W., Hillyard, S.A., Krausz, H.I. and Galambos, R. Human auditory evoked potentials. I. Evaluation of components. Electroenceph. clin. Neurophysiol., 1974, 36: 179–190.

Plonsey, R. Bioelectric Phenomena. McGraw-Hill, New York, 1969.

Rush, S. and Driscoll, D.A. Current distribution in the brain from surface electrodes. Anaesth. Analg. Curr. Res., 1968, 47: 717–723.

Scherg, M. Spatio-temporal modelling of early auditory evoked potentials. Rev. Laryngol. (Bordeaux), 1984, 105: 163–170.

Scherg, M. and Von Cramon, D. Topographical analysis of auditory evoked potentials: derivation of components. In: R.H. Nodar and C. Barber (Eds.), Evoked Potentials, II. Butterworth, Woburn, 1984: in press.

Schneider, M. A multistage process for computing virtual dipolar sources of EEG discharges from surface information. IEEE Trans. biomed. Engng, 1972, 19: 1–12.

Vaughan, Jr., H.G. The analysis of scalp-recorded brain potentials. In: R.F. Thompson and M.M. Patterson (Eds.), Bioelectric Recording Techniques, Part B. Academic Press, New York, 1974: 158–207.

Vaughan, Jr., H.G. The neural origins of human event-related potentials. In: I. Bodis-Wollner (Ed.), Evoked Potentials. Ann. N.Y. Acad. Sci., 1982, 388: 125–138.

Vaughan, Jr., H.G. and Ritter, W. The sources of auditory evoked responses recorded from the human scalp. Electroenceph. clin. Neurophysiol., 1970, 28: 360–367.

Vaughan, Jr., H.G., Ritter, W. and Simson, R. Topographic analysis of auditory event-related potentials. In: H.H. Kornhuber and L. Deecke (Eds.), Motivation, Motor, and Sensory Processes of the Brain. Prog. in Brain Res., Vol. 54. Elsevier, Amsterdam, 1980: 279–285.

Wolpaw, J.R. and Penry, J.K. A temporal component of the auditory evoked response. Electroenceph. clin. Neurophysiol., 1975, 39: 609–620.

Wolpaw, J.R. and Wood, C.C. Scalp distribution of human auditory evoked potentials. I. Evaluation of reference electrode sites. Electroenceph. clin. Neurophysiol., 1982, 54: 15–24.

Wood, C.C. Application of dipole localization methods to source identification of human evoked potentials. In: I. Bodis-Wollner (Ed.), Evoked Potentials. Ann. N.Y. Acad. Sci., 1982, 388: 139–155.

Wood, C.C. and Wolpaw, J.R. Scalp distribution of human auditory evoked potentials. II. Evidence for overlapping sources and involvement of auditory cortex. Electroenceph. clin. Neurophysiol., 1982, 54: 25–38.

Woods, D.L., Knight, R.T. and Neville, H.J. Bitemporal lesions dissociate auditory evoked potentials and perception. Electroenceph. clin. Neurophysiol., 1984, 57: 208–220.